Available online at www.sciencedirect.com
ScienceDirect
Nuclear Instruments and Methods in Physics Research 00 (2017) 01–16
Nuclear Instruments and Methods in Physics Research

Novel Silicon Photomultipliers suitable for Dual-Mirror Small-Sized Telescopes of the Cherenkov Telescope Array Project

G. Romeo[a*], G. Bonanno[a], G. Sironi[b], M.C. Timpanaro[a]

[a]*INAF, Osservatorio Astrofisico di Catania, Via S. Sofia 78, I-95123 Catania (Italy)*
[b]*INAF Osservatorio Astronomico di Brera, via Emilio Bianchi 46, 23807, Merate (LC), (Italy)*

Abstract

Silicon Photomultipliers (SiPMs) for their peculiar characteristics are detectors suitable to be used in cameras for Small-Sized Telescopes (SSTs) proposed for the Cherenkov Telescope Array (CTA). Dual-mirror SST (SST-2M) telescopes have a relatively small plate scale that allows to employ SiPMs relatively small, fairly easily manufactured by silicon foundries.
In CTA, the Night Sky Background (NSB) level of typically 25 MCnts/s/pixel places severe constraints on the trigger capability due to accidental coincidence on neighbouring pixels. In order to suppress such events, it is necessary to reduce Optical Cross-Talk (OCT), a mechanism whereby a single optical photon can produce multiple avalanches in the SiPM, while keeping good Photon Detection Efficiency (PDE). This paper presents the latest characterization results of novel Low Voltage Reverse (LVR) 2nd and 3rd version Multi-Pixel Photon Counter (MPPC) detectors manufactured by Hamamatsu Photonics (HPK), capable to achieve a Photon Detection Efficiency enhancement and an optical cross-talk reduction. Two 7 × 7 mm^2 S14520 LVR2 MPPCs with 75 μm micro-cells have been tested and compared with respect to detectors of same size and 50 μm micro-cells.
A comparative analysis of a 3 × 3 mm^2 S14520 LVR2 and a S14520 LVR3 devices has been also carried out demonstrating that the LVR3 gives better photon detection in the 240 – 380 nm spectral range.
Finally, the effect on the OCT due to a cut off infrared filter has been analysed.

Keywords: Silicon Photomultipliers, Detector Characterization, Photon Detection Efficiency, Optical Cross Talk, Small Sized Telescope, Cherenkov Telescope Array.

1. Introduction

The Cherenkov Telescope Array [1] is a project created to build the next generation ground-based gamma-ray observatory. CTA will build on the strengths of current Imaging Atmospheric Cherenkov Telescopes (IACT), employing three telescope design groupings, the Large-Sized Telescope (LST), Medium-Sized Telescope (MST) and Small-Sized Telescope (SST) arrays to enhance the sensitivity over current facilities by up to an order of magnitude [1] in the 100 GeV to 10 TeV range and extend the accessible energy range from well below 100 GeV to above 100 TeV. The SST array is optimized for sensitivity and coverage from a few TeV to 300 TeV. About 70 SST telescopes are planned to cover several square kilometres in order to achieve the necessary sensitivity. Because of the large number of telescopes required, cost reduction is critical for the SST. However, the camera cost cannot be reduced by simply reducing its size, due to the minimum number of pixels required (>1000) and the relatively high unit cost of traditional photon sensing photomultiplier tubes (PMTs). In order to mitigate this problem, the SST utilizes silicon photomultipliers (SiPMs) as the baseline photon sensor technology [3]. Actually, SiPM detectors with large size (i.e. 20 × 20 mm^2) surely suffer from high dark count rates and very high recovery time. One solution is to make use of dual-mirror optics which have a relatively small plate scale and whose focal plane can be covered with SiPMs with sizes ranging from 6

* *Corresponding author*: Giuseppe Romeo (giuseppe.romeo@oact.inaf.it)

× 6 mm^2 to 7×7 mm^2 [4].

SiPM detectors, thanks to their outstanding characteristics in terms of photon detection efficiency, photon number resolution, low operating voltage, fast dynamic response and insensitivity to magnetic fields, are suitable in the fields of high-energy astrophysics and IACT applications [5]-[13]. Considerable effort is presently being invested by the producers of SiPMs to further improve the global performance achieved by this class of devices[14]-[16], as well as characterization studies and methodologies for evaluating the detector performance have been carried out [17]-[25]. Actually, we can safely assert that the SiPMs PDE is greater than that of PMTs in the 300 - 700 nm spectral range, but another SiPM parameter has to be carefully considered: the optical crosstalk, a mechanism whereby a single optical photon can produce multiple avalanches in the SiPM. In CTA, the night sky background level of typically 25 MCnts/s/pixel places severe constraints on the trigger capability due to accidental coincidence on neighbouring pixels. In order to suppress such events, it is necessary to reduce optical crosstalk at very low level, while keeping good Photon Detection Efficiency.

This paper presents the characterization of a newly available large-area Low Voltage Reverse 2nd and 3rd version multi-pixel photon counter detectors manufactured by Hamamatsu Photonics, capable of achieving a photon detection efficiency enhancement and an optical cross-talk reduction and suitable for the focal plane of the ASTRI Mini-Array Project (Astrofisica con Specchi a Tecnologia Replicante Italiana) [8][8] within the Cherenkov Telescope Array Observatory [1]. In order to show the perfect fitting in the ASTRI camera and the very good global fill factor achieved, a brief description of the relevant mechanical parameters is also provided.

Two 7 × 7 mm^2 S14520 LVR2 MPPCs with 75 μm micro-cells have been tested and a comparative analysis of the large pixel pitch (75 μm) detector versus the smaller pixel pitch (50 μm) device with the same active area is here described.

We also carried out PDE measurements on a 3 × 3 mm^2 S14520 LVR3 MPPC and compared it with an S14520 LVR2 device. The results found demonstrate that the S14520 LVR3 device gives better PDE in the 240 - 380 nm spectral range respect to the S14520 LVR2 SiPM.

The effect of an optics (a cut off infrared filter in the specific case of the ASTRI camera) placed in front of a SiPM on the OCT is described.

The measurements presented here are carried out at the Catania astrophysical Observatory Laboratory for Detectors (COLD) within INAF – Osservatorio Astrofisico di Catania.

2. ASTRI focal plane coverage and SiPM relevant mechanical parameters

The optical configuration of the ASTRI SST-2M telescope permits to design a compact and lightweight camera to be placed at the curved focal surface. The detection surface requires a spatial segmentation with interspace of a few millimetres to be compliant with the imaging resolving angular size (0.19°). In order to match the angular resolution of the optical system, the design of the ASTRI camera has to comply with the dimensions of the single pixel and of the basic detection module (the tile). Since the convex shaped focal surface of the SST-2M camera has a curvature radius of about 1m, the curved surface of the camera has to fit with a certain number of square pixels without losing the required focusing capability of the optical system. This specification is physically accomplished by a pixel of about 7 × 7 mm^2 and a detection module of 57.6 × 57.6 mm^2.

Figure 1 shows the focal plane assembly. 37 detection modules (about 2000 pixels) form the camera at the focal plane; this structure is capable to achieve a full Field of View (FoV) of 9.6°.

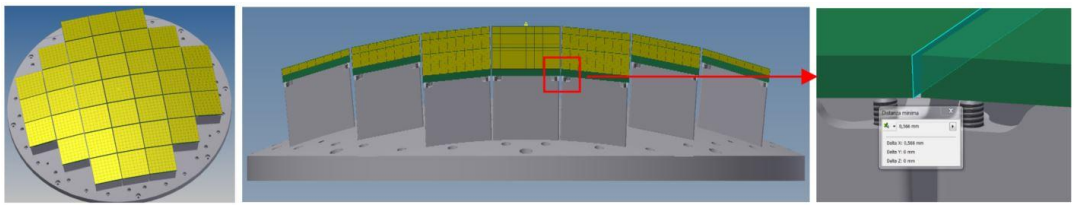

Figure 1. ASTRI camera focal plane assembly. The telescope curved focal plane imposes the arrangement of detection modules and the maximum allowable dimensions of the tiles.

Using 7 × 7 mm^2 SiPM detectors with 75 µm cell as pixels, 93 micro-pixels can take place along the two pixel dimensions giving in total 8649 micro-pixels ensuring a saturation level higher enough of that required by the CTA project. In this case the sensitive area will result 6.975 × 6.975 mm^2 and placing 8 × 8 pixels in one tile we can obtain a total area of 57.4 × 57.4 mm^2 meaning 3294.75 mm^2 and an active area of 3091.36 mm^2 giving a tile filling factor of 93.83%. Figure 2 shows the schematic of tile and the detail of a single 7 × 7 mm^2 pixel.

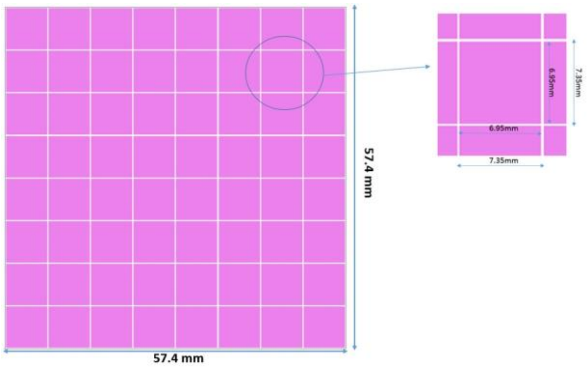

Figure 2. 8 × 8-pixels tile schematics. Using 7 × 7 mm^2 SiPMs 57.4 × 57.4 mm^2 can be assembled. On the right part a detail of a single 7 × 7 mm^2 pixel is shown. With this configuration a total area of 3294.75 mm^2, an active area of 3091.36 mm^2 and a filling factor of 93.83% are achieved.

3. Large-Area Low Voltage Reverse (LVR) 2nd and 3rd version MPPC detectors

The optical trench improvement, started with the Low Cross Talk series MPPC and characterized by new types of trenches that enabled cross-talk reduction, has been continued in the new denominated Low Voltage Reverse family. On the other hand, the fill-factor improvement of the new MPPC series results from a functional optimization of the physical structure of the device (maximization of the active area).

The characterized large-area MPPC described in this paper belongs to the latest device series manufactured by Hamamatsu Photonics, denominated LVR family and reported as the MPPC S14520 LVR2 CS (Silicone Coating) and CN (No Coating) and S14520 LVR3 CS and CN series. These are prototype devices provided by the vendor to the COLD laboratory for testing and evaluation purposes. Figure 3 shows the three characterized devices while Table I reports the main features of the characterized detectors.

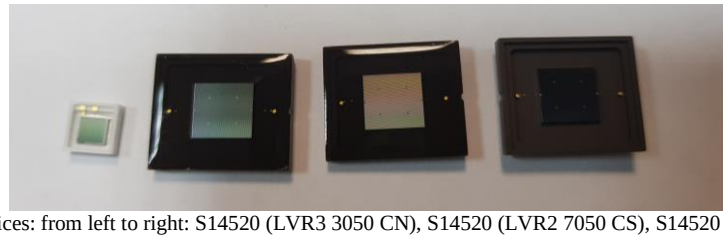

Figure 3. Characterised devices: from left to right: S14520 (LVR3 3050 CN), S14520 (LVR2 7050 CS), S14520 (LVR2 7075 CS) and. S14520 (LVR2 7075 CN)

TABLE I

Main physical features of the characterized MPPC detectors

device series	S14520(LVR2 7075 CS)	S14520(LVR2 7075 CN)	S14520(LVR2 7050 CS)	S14520 (LVR3 3050 CN)
cell pitch	75 μm	75 μm	50 μm	50 μm
device size	7 × 7 mm^2	7 × 7 mm^2	7 × 7 mm^2	3 × 3 mm^2
sensitive area	6.975 × 6.975 mm^2	6.975 × 6.975 mm^2	6.950 × 6.950 mm^2	3.00 × 3.00 mm^2
microcells	8649	8649	19321	3600
surface coating	Silicone resin	No coating	Silicone resin	No coating
fill-factor	82%	82%	74%	74%
breakdown voltage*	38.00V	38.60V	38.20V	38.68V

* at 25°C

4. Characterisation Setup

The electro-optical equipment used for SiPM measurements is depicted in Figure 4.

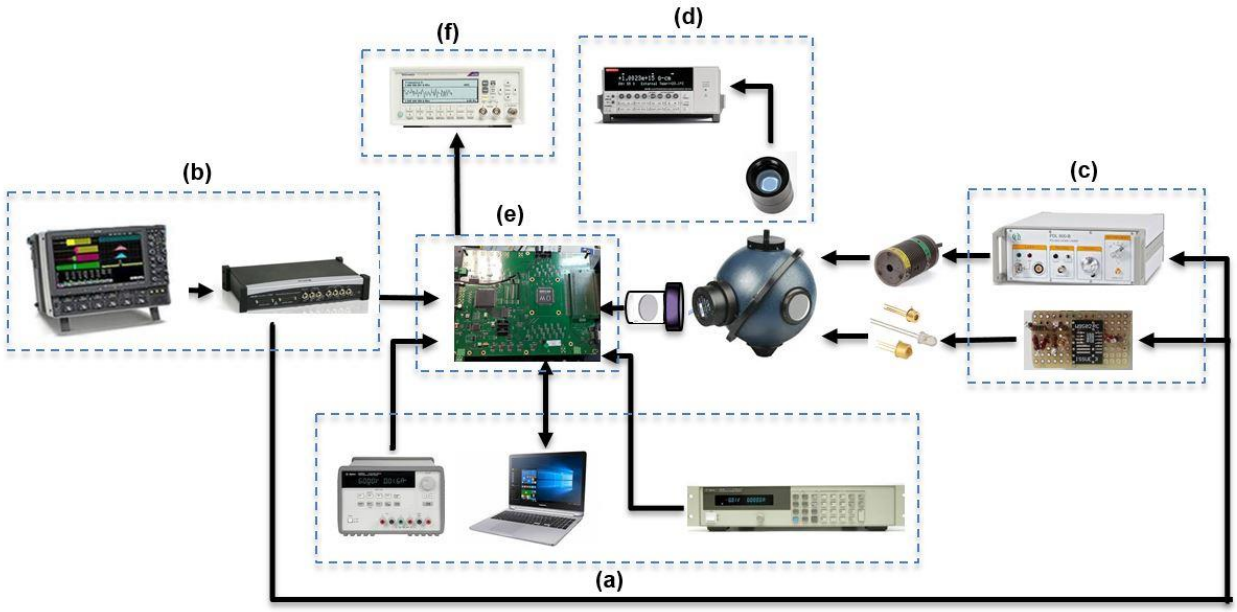

Figure 4. Characterization setup based on pulsed light sources: lasers and LEDs. Apart the integrating sphere, that can be considered the central part of the system 5 main blocks can be envisaged: a) power supply, b) pulse generator, c) laser and LED drivers, d) calibrated reference photodiode, e) CITIROC-1A electronic front-end, f) counter.

Along the schematic, five main blocks can be envisaged:

a) SiPM and electronic front-end power supply: constituted by an Agilent 6634B to supply the high voltage to the SiPM and an Agilent E3631A to supply the voltage levels to the LED driver.

b) Pulse generator: constituted by an oscilloscope LeCroy wavePro 725Zi 2.5GHz and a pulse generator LeCroy ArbStudio 1104 to generate the synchro signals for the pulsed light source.

c) Laser and LED controllers: constituted by a PicoQuant PDL 200-B to drive the lasers and an appropriate electronic circuit based on an AD8009 ultra-fast amplifier, capable of conditioning signals at a slew rate of 5.5V/μs (545ps rise time).

d) Calibrated reference detector: constituted by an IRD photodiode NIST traceable and a Keithley 6514 electrometer to measure the photo-current form the reference detector.

e) CITIROC-1A electronic front-end: to drive and process the SiPM signals.

f) Counter Tektronics FCA 3000: to measure the dark count rate for the staircase

Furthermore, a set of calibrated neutral density filters ND30B, ND20B, ND13B and ND10B by Thorlabs[1] are used in front of the SiPM to attenuate the signal and avoid to work with luminous level that could saturate the detector, while having sufficient current signal detected by the photodiode.

The apparatus allows PDE measurements in the spectral range of 280 – 850 nm by using 18 pulsed light sources.

The wavelength of each source is reported in Table II.

TABLE II

Pulsed light sources and their respective wavelength available at the COLD laboratory

Identifier code	Wavelength [nm]	Type
LED285W	285	LED
LED315W	315	LED
LED341W	341	LED
LED385L	385	LED
LDH-P-C-405	405	Laser
LED430L	430	LED
EPL-450	450	Laser
LED-450	450	LED
LED465E	465	LED
PLS-8-2-746	496	LED
LED505L	505	LED
LED525L	525	LED
LED570L	570	LED
LED591E	591	LED
LDH-P-635	635	Laser
LED660L	660	LED
LED680L	680	LED
LED780E	780	LED
LED851L	851	LED

Temperature control and stabilization (± 0.5°C) is obtained through a dedicated thermoelectric cooling system based on a Peltier cell; the entire cooling system is thermally calibrated and can achieve temperatures from 2°C to 30°C. The mechanical housing is able to host various types of detectors by simply using a dedicated electronic adapter board.

As stated above, the main element of the front-end electronics for SiPM characterization is the Cherenkov Imaging Telescope Integrated Read-Out Chip (CITIROC) [26], which is an advanced version of the Extended Analogue SiPM Integrated Read-Out Chip (EASIROC) [27], both produced by WEEROC[2]. The chip has been selected as the front-end electronics for the ASTRI Mini Array camera. The analog core of the chip has 32 channels, each one incorporating:

- An analog-to-digital converter (ADC) for the SiPM high voltage adjustment.
- Two preamps that allow settling dynamic range, through variable capacitors, between 160 fC and 320 pC.
- A trigger line consisting of two fast shapers and two discriminators.
- Two slow shapers and two track and hold blocks are responsible for measurement of the Pulse Height Distribution (PHD).

The block diagram of one channel is shown in Figure 5.

[1] https://www.thorlabs.com/navigation.cfm?guide_id=2185
[2] http://www.weeroc.com

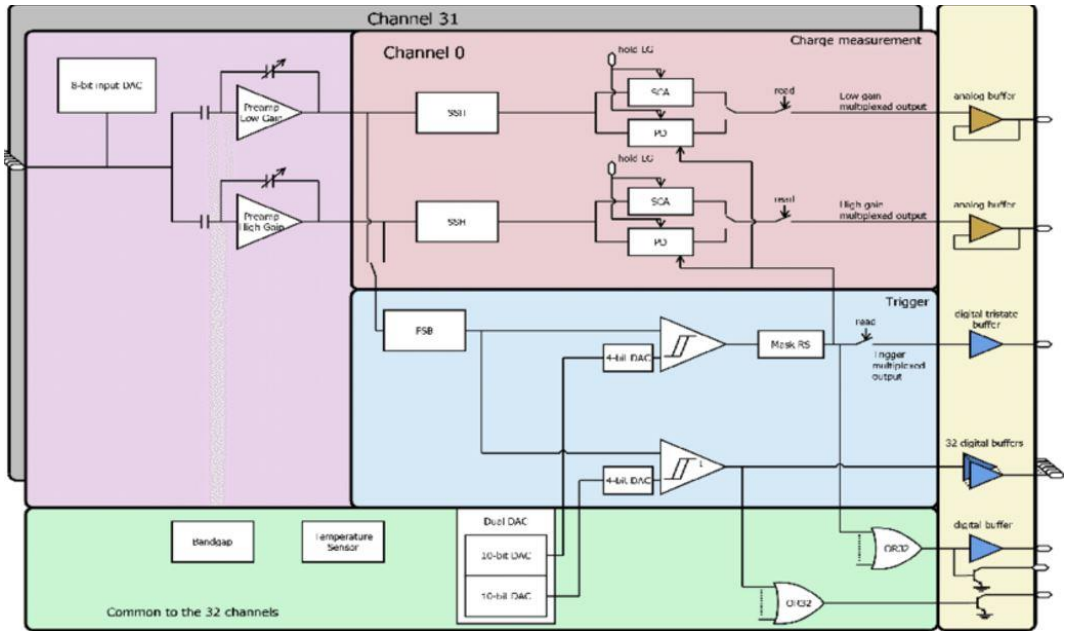

Figure 5. CITIROC-1A single channel block diagram.

The part of the ASIC chip used to obtain staircase measurements is depicted in Figure 6. The SiPM pulse is amplified by the High Gain (HG) preamplifier and then is shaped (15 ns shaping time) by the bipolar fast shaper. A discriminator with a programmable threshold (10 bit DAC) is used to drive the output signal through the OR32, and in turn, to drive the counter Tektronics FCA 3000.

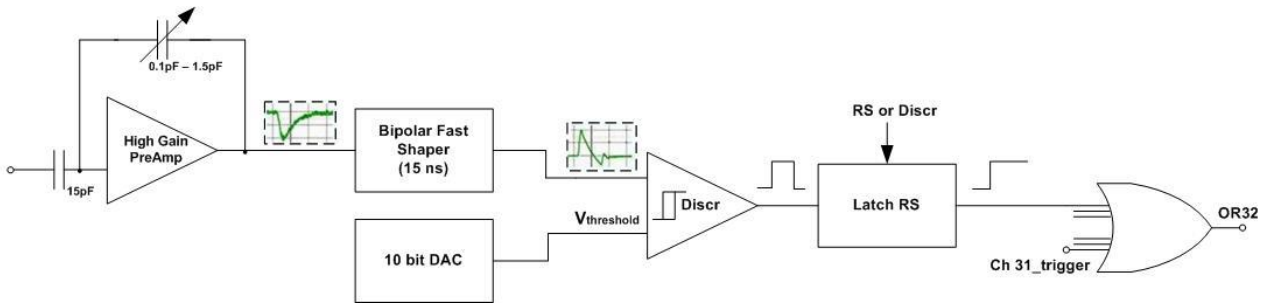

Figure 6. Block diagram of the used electronics inside the ASIC for staircase measurements.

As we will discuss later, the 15 ns shaping time of the bipolar fast shaper, and in general the bandwidth of the input circuit is responsible for an OCT increase due to the inadequate Pole Zero Cancellation (PZC) that lead to a sort of pile-up effect in the sense that the DCR at 0.5 p.e. threshold is lower than that effective as well as the DCR at 1.5 p.e. is higher than the real one.

5. Experimental results

Based on the above mentioned equipment, experimental measurements on the S14520 LVR2 series 7 × 7 mm^2 MPPC are carried out and presented here in terms of the main detector performance parameters, i.e. Dark Count Rate (DCR), Optical Cross-Talk and Photon Detection Efficiency. In particular, the PDE has been measured in the 285 – 850 nm spectral range and at 405 nm at various operating voltages.

A. Dark Count Rate and Optical Cross-Talk

The Dark Count Rate is essentially defined as the count rate of avalanche pulses produced by primary (uncorrelated) carriers, resulting in events that are perfectly equivalent to the signal from real photons.

SiPM optical cross-talk, as reported in literature ([17][18][19],[22]-[25]), is evaluated as the ratio of the DCR at 1.5 p.e. (photon equivalent) with respect to that at 0.5 p.e. This approach is based on the assumption that the probability of triggering two uncorrelated avalanches at the same time is negligible.

Figure 7 shows the DCR curves (also known as staircase functions) for the characterized SiPMs S14520 (LVR2 7075 CS) and S14520 (LVR2 7975 CN) as a function of the discriminator threshold at 3°C operating temperature and for over-voltage values from 2-V up to 5-V, in steps of 1-V. For a threshold above the electronics noise, all thermally generated avalanches are counted as a single pulse, as well as tunnel-assisted generated charge, afterpulsing and indirect optical cross-talk (extra-charge noise).

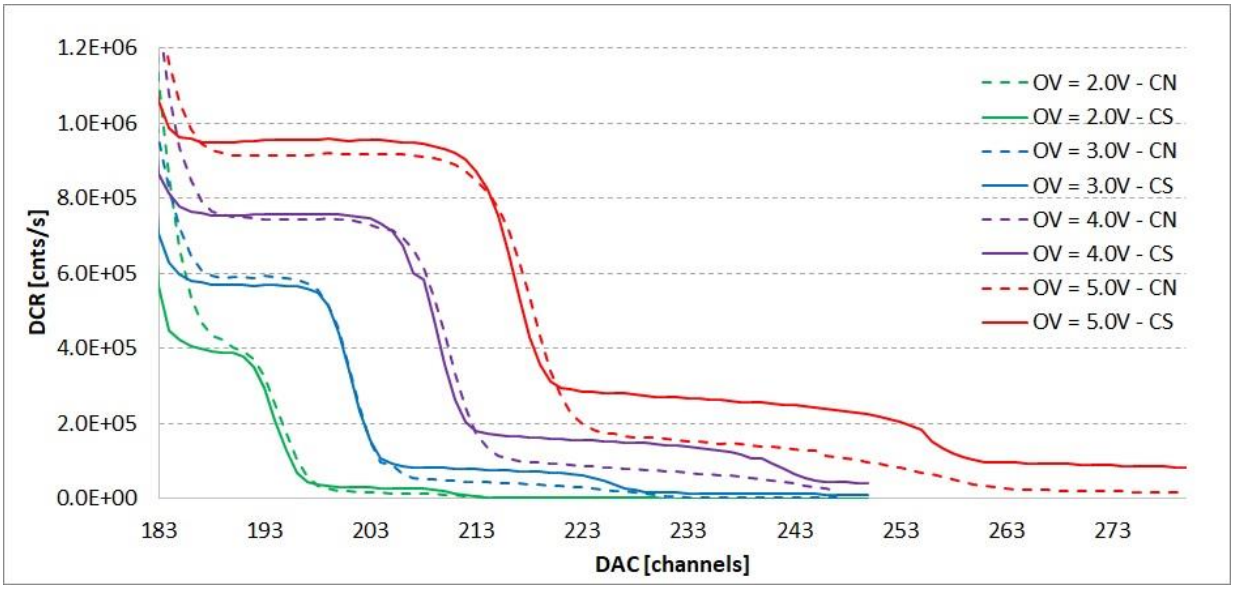

Figure 7. DCR curves for the characterized S14520 (LVR2 7075 CS) and S14520 (LVR2 7075 CN) detectors as a function of the discriminator threshold at 3°C operating temperature. The difference in the second p.e. is clearly evident and implies a reduced OCT in the CN series device.

The staircase functions have been carried out at 3°C because an OCT probability dependency from the DCR has been observed during measurements. At DCR higher than about 700 KCnts/s a sort of pile-up effect occurs, giving a DCR underestimation at 0.5 p.e. (photon equivalent) and overestimation at 1.5 p.e., thus distorting the final OCT values. In large devices the effect is more pronounced due to the higher DCR. As this last depends from temperature, we measured the OCT at 3.0V over-voltage of 3 × 3 mm^2, 6 × 6 mm^2 and 7 × 7 mm^2 LVR2 devices by varying the operating temperature. In Figure 8 it can be observed that, in the analysed temperature range, the OCT of the 3 × 3 mm^2 device remains at about 2.0% in all the range, meaning that the DCR (about 300 KCnts/s at 20°C) is sufficiently low to avoid the pile-up effect, while the other two devices suffer from the effect and at temperatures higher than 5°C, at which the DCR is 700 KCnts/s and 850 KCnts/s respectively for the 6 × 6 mm^2 and 7 × 7 mm^2, the OCT increases proportionally to the temperature essentially because the DCR increases. Below 5°C we observe, as expected, that the OCT depends only by the SiPM size. The explanation of this behaviour, as stated above, has to be searched in the front-end electronics input circuit that operates an inadequate PZC.

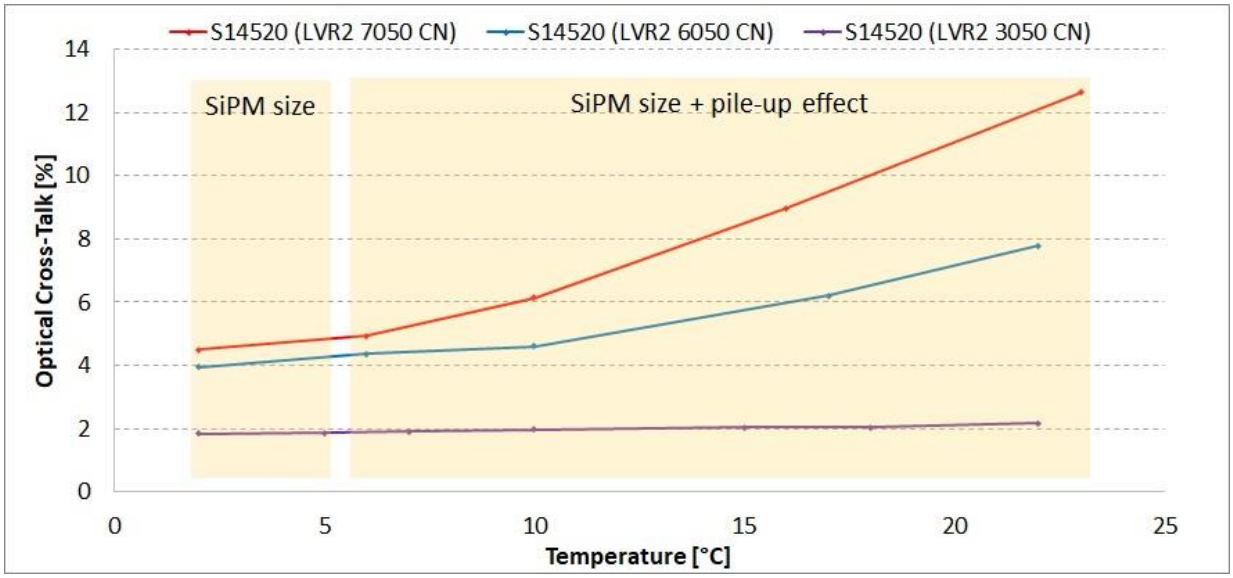

Figure 8. OCT versus temperature. Below 5°C, the OCT depends only by the SiPM size while above 5°C the OCT is affected by the pile-up effect, or better to say the electronic front-end operates an inadequate PZC.

From the obtained staircases depicted in Figure 7 we derived the OCT plots for both CS and CN devices and showed in Figure 9. In this figure we also report the OCT versus over-voltage at 15°C because this is the ASTRI camera working temperature. From measurements we can derive the degradation of OCT when we operate the camera at 15°C.

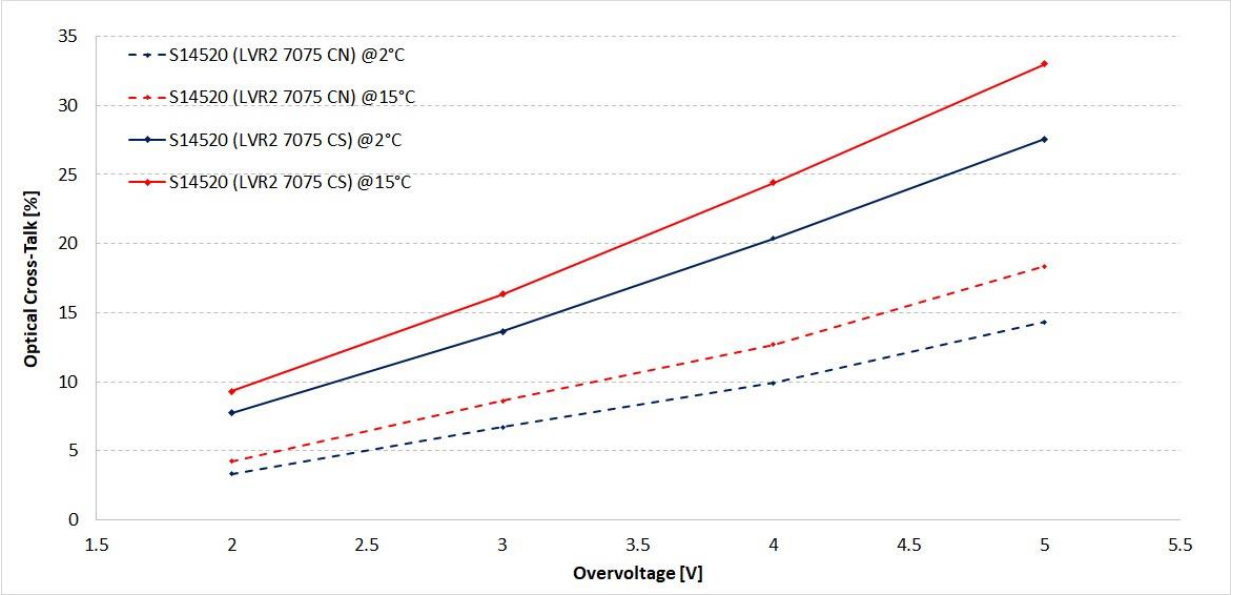

Figure 9. OCT versus overvoltage at 2°C and at 15°C. The CN series shows a lower OCT respect to the CS series because the protective coating in the CS series. The electronics is responsible for the different behaviour at the two temperatures.

As easily understood by the staircases of Figure 7 and as expected the CN series shows a lower OCT than the CS series. This is essentially due to the protective resin coating on top the SiPM sensitive surface that operates a back reflection of the photons produced during an avalanche. A higher OCT at 15°C is observed because the pile-up effect due to the inadequate PZC of the electronics. The OCT of the SiPM S14520 (LVR2 7075 CS) is about double respect to that of the CN series, while an OCT increasing of about 2.0% is observed at an operating temperature of 15°C.

B. Photon Detection Efficiency

SiPM absolute PDE measurements are based on the statistical analysis of the pulse heights distribution of the SiPM devices both in light and in the dark conditions, by which the number of pulses per unit time in monochromatic light conditions are compared to the light level recorded by a reference NIST photodetector at the same time. The used technique was widely discussed in [20].

The adopted photon counting technique for determining the detector PDE is insensitive to the optical cross-talk, as we measure the probability of detecting 0 photons and derive the average assuming the Poisson statistics. The average number of photons revealed by the SiPM is given by:

$$\overline{N}_{SiPM} = -ln\left[\frac{N_{ped}}{N_{ped}{}^{DK}}\right]$$

Where:

N_{ped} is the number of events at 0p.e. (that is the pedestal) with light source.

$N_{ped}{}^{DK}$ is the number of events at 0p.e. (that is the pedestal) without light source (Dark).

From the other side the average number of photons revealed by calibrated photodiode $\overline{N}_{ph\ cal\text{-}Diode}$ is given by:

$$N_{ph\ Cal-Diode} = \frac{N_e}{QE(\lambda)}$$

With N_e the number of photoelectrons detected by the calibrated photodiode and $QE(\lambda)$ its Quantum Efficiency.

The PDE is then obtained by the ratio:

$$PDE = \frac{\overline{N}_{SiPM}}{\overline{N}_{ph\ Cal-Diode}} \times \frac{A_{Diode}}{A_{SiPM}}$$

Where A_{Diode} and A_{SiPM} are the areas of both detectors, because we don't use diaphragms.

However, it has to be observed that the obtained PDE is not immune to extra-charge noise (indirect cross-talk and afterpulsing), and therefore may be slightly overestimated.

We measured the PDE as a function of the over voltage for the wave-length of 405 nm. To check the improvement of the S14520 (LVR2 7075 CS and CN) respect to the MPPC of same series but with 50 mm micro-cell, we also measured the PDE versus the over-voltage of the S14529 (LVR2 7050 CS and CN). Figure 10 shows the compared PDEs.

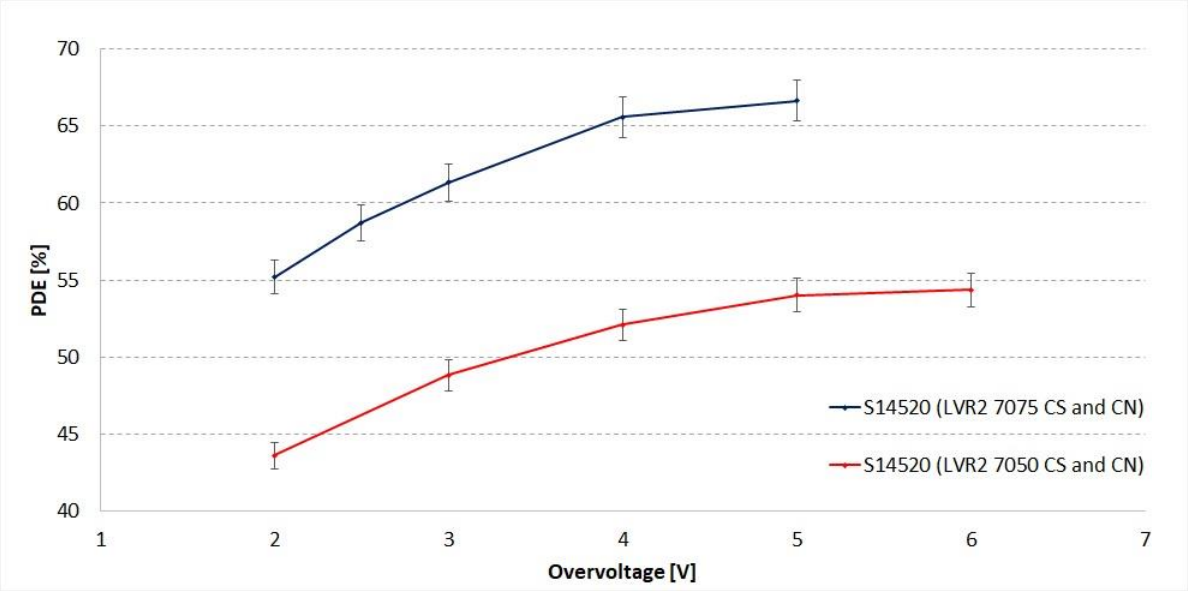

Figure 10. OCT versus over-voltage at 405-nm. Comparison between S14520 (LVR2 7075 CS and CN) and S14520 (LVR2 7050 CS and CN).

As can be noted, the S14520 (LVR2 7075 CS and CN) reaches the PDE saturation of about 67% at 5.0V of over voltage, while the S14520 (LVR2 7050 CS and CN) at the same over voltage saturates at 48%, and the difference of about 10% is maintained at all the over voltage in the 2.0 - 6.0V range.

PDE measurements in the 310 – 850 nm wavelength range of the S14520 (LVR2 7075 CN) and S14520 (LVR2 7075 CS) have been obtained by using the pulsed sources (lasers and LEDs) described in section 4 and are reported in Figure 11. The measurements have been carried out by operating the detectors at over voltages of 3.0V and 4.0V, moreover, the PDE of the S14529 (LVR2 7050 CS) and S14520 (LVR2 7075 CN) has been measured and reported on the plot to better evaluate the achieved performance of the SiPM with larger microcells.

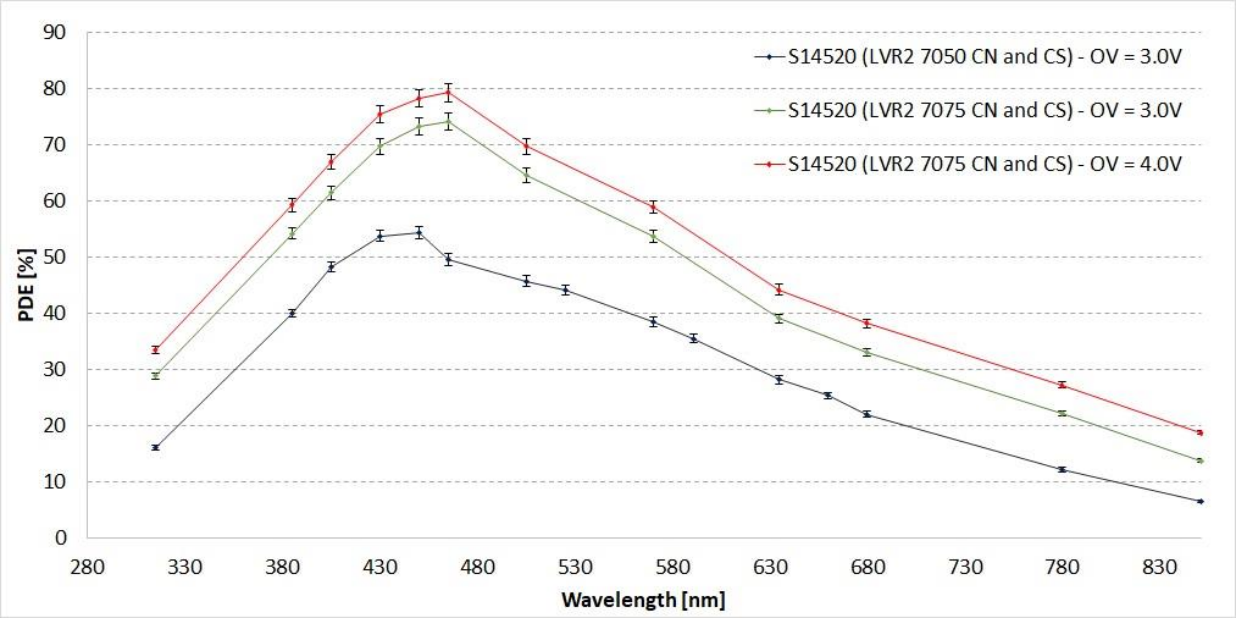

Figure 11. *PDE* measurements of the characterized S14520 (LVR2 7075 CS) and S14520 (LVR2 7075 CN) detectors at 3.0V and 4.0V over voltage are carried out in the 310 – 850 nm spectral range. The PDE of S14520 (LVR2 7050 CS) and S14520 (LVR2 7050 CN) at 3.0V over voltage is also added for comparison. A PDE of 74% at 3.0V over-voltage is achieved at wavelengths in the range 460 – 470 nm and 78% at 4.0V over-voltage, where a reasonable OCT is measured.

In the spectral range 460 - 470 nm a PDE of 74% at 3.0V over voltage is achieved. A considerable PDE difference between the two kinds of SiPM 50 µm and 75 µm micro-pixel pitch is observed. At 4.0V over-voltage, where the trig-

ger probability is about 97%, a PDE of 78% has been measured, that is compatible with a fill factor of 84% and a Quantum Efficiency of about 95%. The impressive PDE and the relatively low OCT lay the basis for having a suitable 7×7 mm^2 SiPM for the SST dual mirror telescope of the CTA project.

In order to better quantify the detectors performance, PDE measurements at 405 nm as a function of OCT (at 2°C operating temperature) for both CN and CS series devices are depicted in Figure 12.

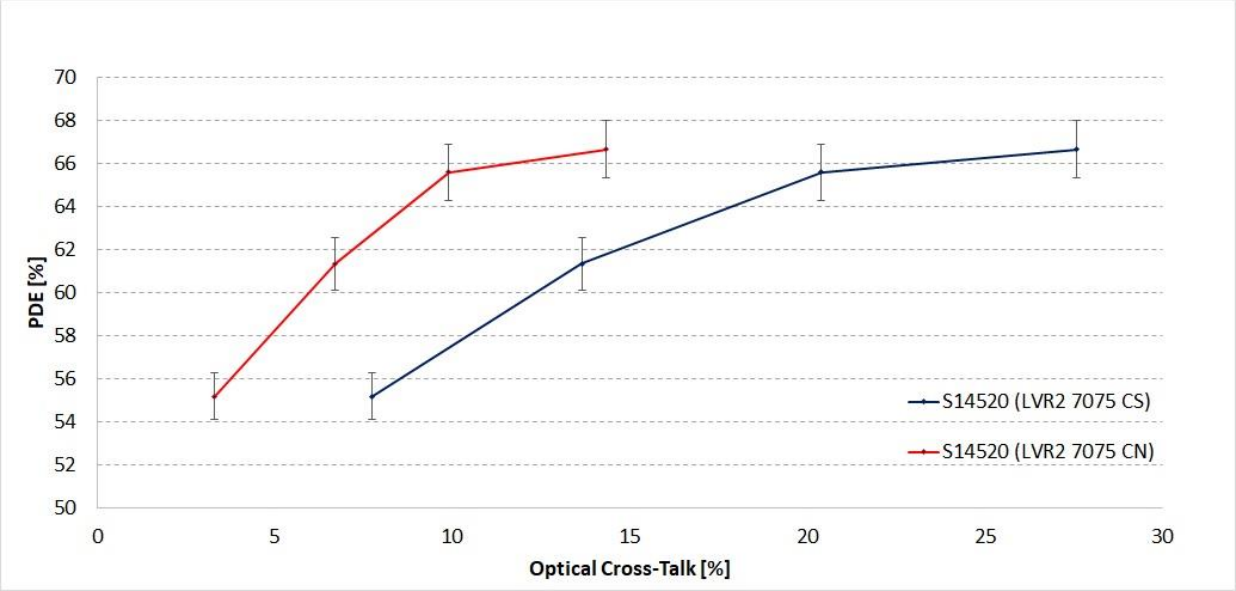

Figure 12. PDE(405nm) versus the applied overvoltage for the S14520 (LVR2 7075 CS) and S14520 (LVR2 7075 CN) detectors. As can be noted, a PDE higher than 60% is achievable with only 6.5% of OCT in the CN series MPPC and with 13.5% of OCT in the CS series detector.

Such plots allow an evaluation of the optimal trade-off between PDE and optical cross-talk for the specific application. Data points in Figure12 refer to the same overvoltage values as in Figure 10.

As can be observed, at over voltages of 3.0V, a PDE higher than 60% is achieved and OCT of only 6.5% in the CN series MPPC and 13.5% CS series detector. As discussed in the previous subsection, the S14520 (LVR2 7075 CS) MPPC device gives greater optical cross-talk due to the coating, at 2.0V of over voltage the OCT can be reduced to about 7.0% but at expenses of the PDE that drops to about 56%. In applications where a OCT of ~15% is acceptable, a PDE of ~60% can be achieved by the CS series device while the CN series MPPC is preferable where low cross-talk values are required. Of course the CN devices require a more accurate handling and increase breakage risks.

C. Relative PDE of the LVR3 respect to the LVR2

The HPK made an effort to also improve the SiPM response in the 300 – 350 nm spectral range. They produced another series named LVR3 that takes into account the improvement. We received from HPK only a 3×3 mm^2 with 50 µm microcell LVR3 device with no coating S14520 (LVR3 3050 CN). We measured the PDE of this device and compared with that of an LVR2 device (same dimensions and microcell). Figure 13 shows the PDE versus wavelength in the 280 – 850 nm range obtained by operating both devices at 3.0V of over-voltage. A peak in PDE of about 55% is measured in the 430 – 450 nm range for both devices while at 285 nm the S14520 LVR3 shows a 27% of PDE and the S14520 LVR2 gives a PDE of 20%. A similar behaviour but with a slightly difference is achieved at 315 nm and 385 nm.

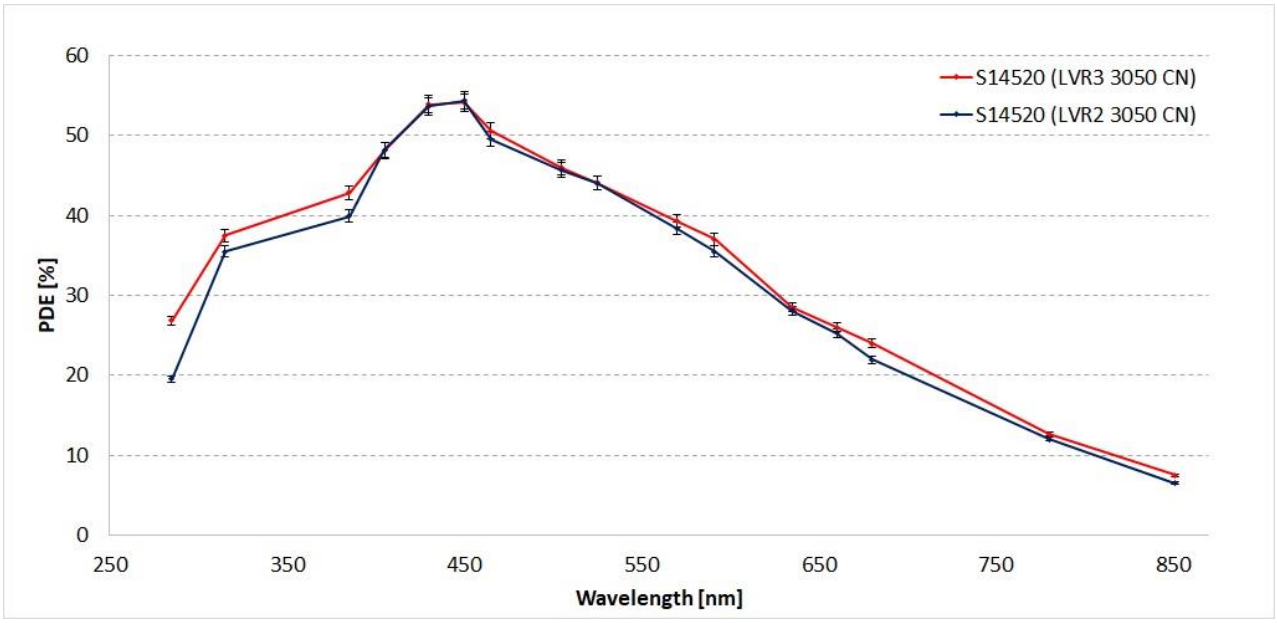

Figure 13. S14520 LVR2 and S1520 LVR3 PDE curves superimposed. The difference in the near UV region is clearly evident

To emphasize the difference between the two technologies we plotted in Figure 14 the ratio of the PDE values obtained for the two devices that in other terms we evaluated the relative PDE

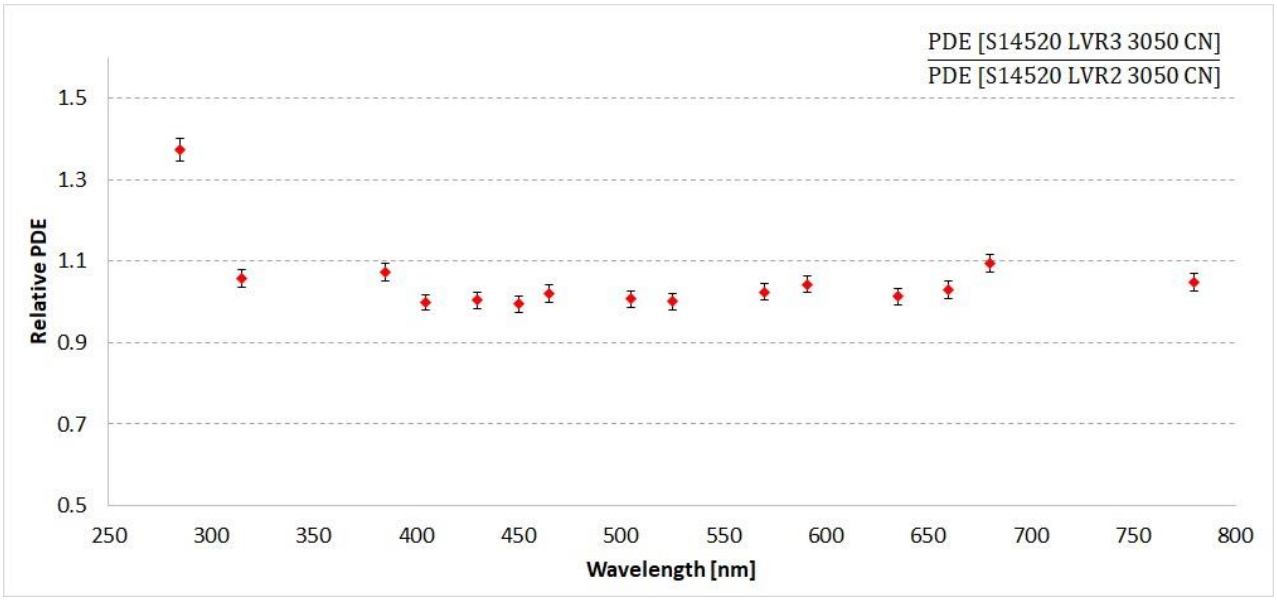

Figure 14. Relative PDE of the S14520 (LVR3 3050 CN) respect to the S14520 (LVR2 3050 CN).

6. Effect of the ASTRI IR Filter on the Optical Cross Talk

As stated above, the ASTRI telescope focal plane is populated with SiPM detectors that have a very good sensitivity in the blue spectral range (where the Cherenkov light emission peaks). Unfortunately, SiPM detectors, being essentially silicon sensors, are also sensitive in the infrared energy band where the emission of the NSB is high.

As a consequence the signal on the SiPM sensor would be due to both the Cherenkov sources and night sky background emissions. To attenuate as much as possible the contribution coming from the latter, it has proposed to introduce a infrared (IR) filtering window on the optical path. The IR filter has been designed to cut the signal at wavelength above 550 nm and would be placed in front of the detectors, working both as filter and as protective window for the SiPM sensors.

The IR filter was implemented as a series of three double coated substrates. This solution allows to reach high contrast, limiting the number of deposited layers. The substrates were realized as circular Spectrosil foils with a diameter of 400-mm and thickness of 1.5 mm. Each coating is realized as ZrO_2-MgF_2 multilayer.

To test the filtering efficiency of the ASTRI filtering window a demonstrator filter was realized. Three small Spectrosil samples were double coated and assembled as in the ASTRI filtering window configuration. The demonstrator filter transmittance was measured in the 330 – 930 nm spectral range with steps of 50 nm. Moreover, since in the ASTRI telescope configuration the detector is hit by photons coming from a wide range of incidence angles, the measurement was repeated for incidence angles from 10 degrees to 50 degrees. The transmittance curves measured for the different incidence angles, and the one corresponding to the calculated mean incidence angle on the filter (44 degrees) are illustrated in Figure 15. A drop off of about 70% is achieved at wavelengths greater 700 nm.

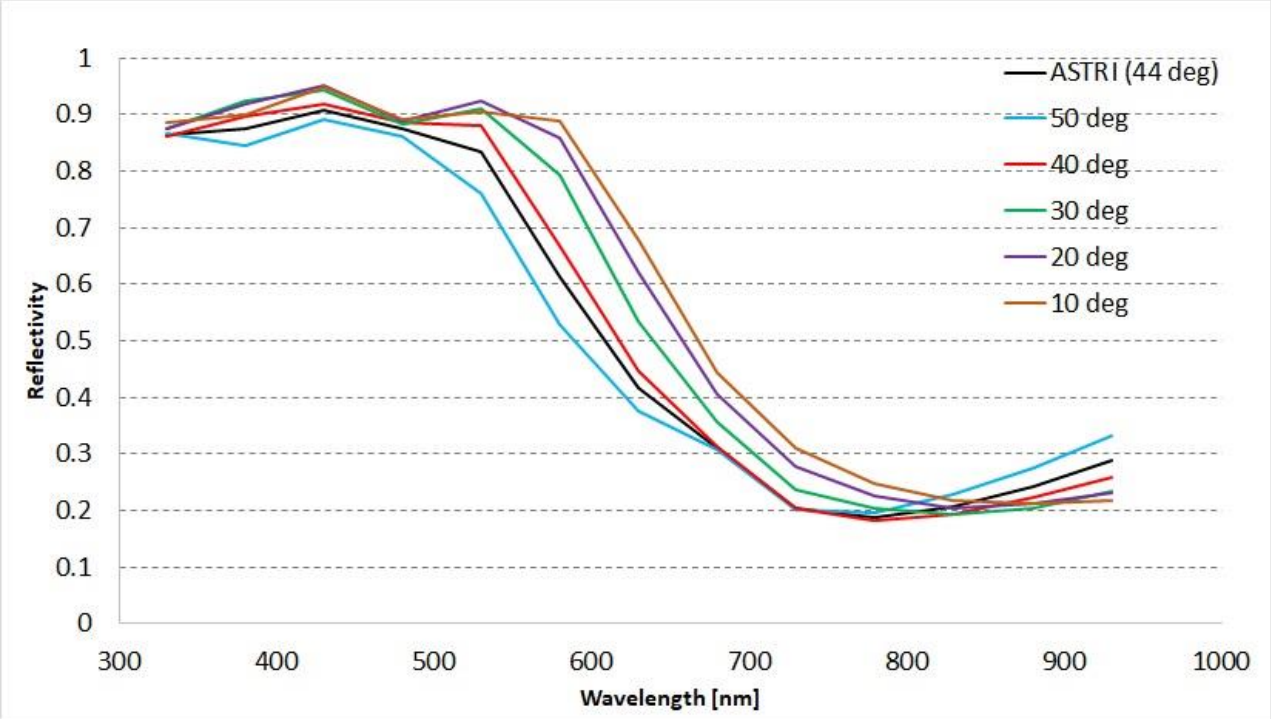

Figure 15. Transmittance in the 300 – 900 nm spectral range at various incident angles of the ASTRI IR filter.

As discussed in section 5, the OCT not only depends on the internal detector features (i.e trenches) and operating conditions (over-voltage) but also on the coating on top of the sensitive area that is responsible for the photons reflection. By extrapolating this behavior to an optics placed close to the detector we can expect an increase of OCT, and also a dependency of the distance from the SiPM has to be accounted because at certain distances the reflection could be negligible: the smaller the distance, the greater OCT. Figure 16 depicts the tiles placement inside the ASTRI camera.

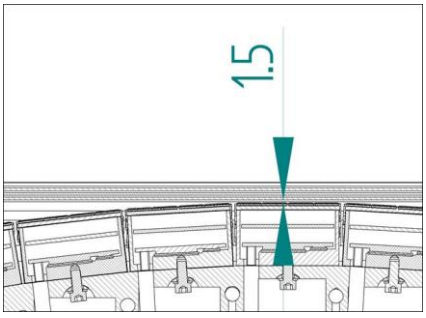

Figure 16. Minimum distance between extrados and intrados of the first sheet of Spectrosil.

As can be noted the SiPM distance from the filter reaches its minimum of 1.5 mm in the central part of the focal plane. Besides the curved focal plane implies a non-constant distance of the pixels from the filter and a rising OCT from the peripheral to the central pixels has to be taken into account.

We used a small reproduction of the filter and by means of appropriate mechanical supports and spacers specially designed for the measurement, we were able to place the sample at 1 mm, 4 mm and 7 mm away from the detector.

Figure 17 shows the measured OCT versus over voltage of the S14520 (LVR2 7075 CN) at the mentioned distances from the detector. For comparison, the OCT obtained without the filter is also reported.

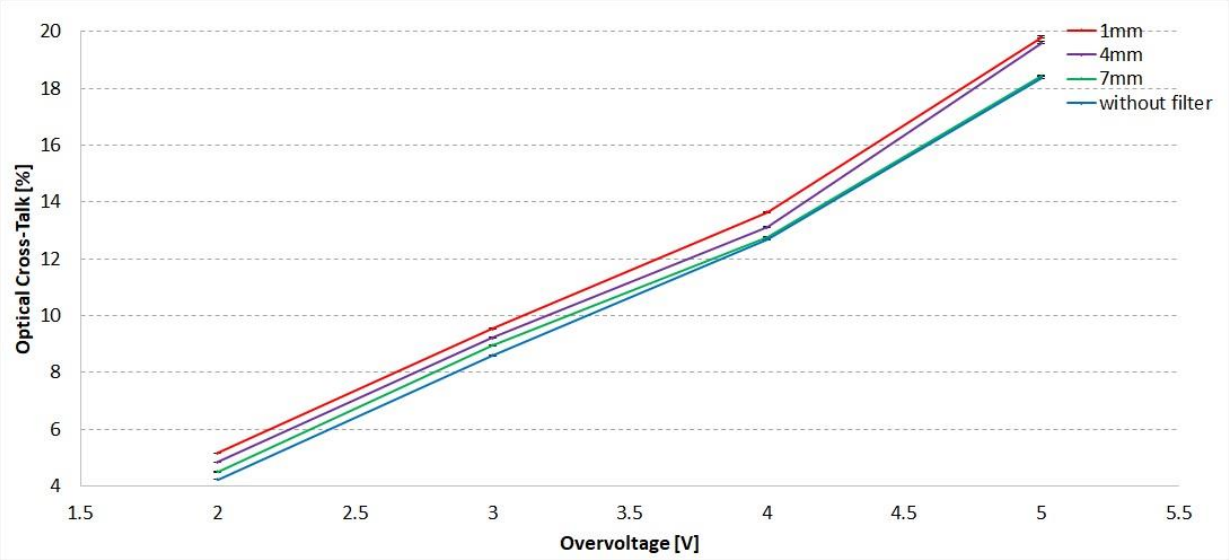

It is evident that the OCT decreases with increase distance between the filter and the SiPM. At distances greater or equal to 7 mm the filter effect is negligible on the OCT increase. In particular, the measurement carried out at 3.0V of over voltage shows that at a distance of 1 mm the OCT increases of about 1.0% while at 4 mm of about 0.6%. The OCT doesn't change when the filter is 7 mm away from the sensitive surface. The S14520 (LVR2 7075 CN) behaves the same way. Thus we can conclude that to avoid the influence of the filter on the OCT the filter has to be placed at a distance greater than 6 mm.

7. Conclusions and Outlook

In this paper, measurement results of a newly available large-area MPPC detectors are reported and discussed. Compared to previous S13360 LCT MPPC series, the new S14520 LVR2 series achieve a significant optical cross-talk reduction due to optical trench improvements, and higher photon detection efficiency, due to geometrical fill-factor enhancement. In addition, we demonstrated that the S14520 LVR3 series offer improved photon detection capabilities in the near ultraviolet (NUV) spectral region, contributing to make the 7×7 mm^2 with 75 µm microcell MPPC particularly suitable for Dual-Mirror Small-Sized Telescopes of the CTA project. Measurement results show that, even for large area devices, promising performance in terms of OCT and PDE is achieved. The OCT has been treated in great detail. The measurements have shown that OCT could be affected by the readout electronics if not properly adjusted. Finally, the investigation of the use of an optics (in the specific case an IR filter) in front of the device has been also reported. The measurements results demonstrated an OCT increase when the SiPM detector is close to the optics.

Acknowledgements

This work is supported by the Italian Ministry of Education, University, and Research (MIUR) with funds specifically assigned to the Italian National Institute of Astrophysics (INAF) for the Cherenkov Telescope Array (CTA), and by the Italian Ministry of Economic Development (MISE) within the "Astronomia Industriale" program. We acknowledge support from the Brazilian Funding Agency FAPESP (Grant 2013/10559-5) and from the South African Department of Science and Technology through Funding Agreement 0227/2014 for the South African Gamma-Ray Astronomy Programme. We gratefully acknowledge financial support from the agencies and organizations listed here: http://www.cta-observatory.org/consortium_acknowledgments.

References

[1] B.S. Acharya, *et al.*, "Introducing the CTA Concept", *Astroparticle Physics*, vol. 43, pp. 3-18, 2013.

[2] M. Actis, *et al*, "Design concepts for the Cherenkov Telescope Array CTA: an advanced facility for ground-based high-energy gamma-ray astronomy", *Experimental Astronomy* 32 (2011) 193-316. arXiv:1008.3703, doi:10.1007/s10686-011-9247-0.

[3] T. Montaruli, *et al*, "The small size telescope projects for the Chrenkov Telescope Array", in*: 34th International Cosmic Ray Conference (ICRC2015),* Vol. 34 of International Cosmic Ray Conference, 2015, p. 1043. arXiv:1508.06472.

[4] G. Pareschi, *et al.*, "The Dual-Mirror Small Size Telescope for the Cherenkov Telescope Array", *Proceedings ICRC '13*, Rio De Janeiro, Brazil, 2013.

[5] O. Catalano, *et al.*, "The Camera of the ASTRI SST-2M Prototype for the Cherenkov Telescope Array", *Proc. SPIE '14, Ground-based and Airborne Instrumentation for Astronomy V*, vol. 91470D, Montreal, Canada, 2014.

[6] S. Siefert, *et al.*, "Ultra Precise Timing with SiPM-Based TOF PET Scintillation Detectors", *Proc. IEEE Nuclear Science Symposium Conference Records*, pp. 2329-2333, 2009.

[7] N. Otte, *et al.*, "The SiPM – A new Photon Detector for PET", *Nuclear Physics B – Proceedings Supplements*, vol. 150, pp. 417-420, 2006.

[8] S. Vercellone, *et al.*, "The ASTRI Miny-Array Science Case", *Proceedings ICRC 2013*, Rio De Janeiro, Brazil, July 2013.

[9] A. Bouvier, *et al.*, "Photosensor Characterization for the Cherenkov Telescope Array: Silicon Photomultiplier versus Multi-Anode Photomultiplier Tube", *Proc. SPIE, Hard X-Ray, Gamma-Ray, and Neutron Detector Physics XV*, vol. 8852, San Diego, USA, 2013.

[10] H. Anderhub *et al.*, "Design and operation of FACT - the first G-APD Cherenkov telescope", *Journal of Instrumentation*, vol. 8, P06008, 2013.

[11] P. La Rocca, *et al.*, "Fabrication, Characterization and Testing of Silicon Photomultipliers for the Muon Portal Project", *Nuclear Instruments and Methods in Physics Research A*, vol. 787, pp. 236-239, 2015.

[12] D. Mazin, *et al.*, "Towards SiPM camera for current and future generations of Cherenkov telescopes", *Proceedings ICRC '13*, Rio De Janeiro, Brazil, 2013.

[13] F. Riggi, "An Extensive Air Shower Trigger Station for the Muon Portal Detector", *Nuclear Instruments and Methods in Physics Research A*, vol. 764, pp. 142-149, 2014.

[14] C. Piemonte, *et al.*, "Characterization of the First Prototypes of Silicon Photomultiplier Fabricated at ITC-irst", *IEEE Transactions on Nuclear Science*, vol. 54, no. 1, pp. 236-244, 2007.

[15] K. O'Neill, *et al.*, "SensL B-Series and C-Series silicon photomultipliers for time-of-flight positron emission tomography", *Nuclear Instruments and Methods in Physics Research A*, vol. 787, no. 1, pp. 169-172, 2015.

[16] B. Dolgoshein, *et al.*, "Large area UV SiPMs with Extremely Low Cross-Talk", *Nuclear Instruments and Methods in Physics Research A*, vol. 695, pp. 40-43, 2012.

[17] G. Bonanno, *et al.*, "Advances in Multi-Pixel Photon Counter Technology: First Characterization Results", *Nuclear Instruments and Methods in Physics Research A*, vol. 806, pp. 383-394, January 2016.

[18] G. Bonanno, *et al.*, "Characterization Measurements Methodology and Instrumental Set-up Optimization for New SiPM Detectors - Part II: Optical Tests", *IEEE Sensors Journal*, vol. 14, no. 10, pp. 3567-3578, 2014.

[19] G. Bonanno, *et al.*, "Characterization Measurements Methodology and Instrumental Set-up Optimization for New SiPM Detectors - Part I: Electrical Tests", *IEEE Sensors Journal*, vol. 14, no. 10, pp. 3557-3566, 2014.

[20] P. Eckert, *et al.*, "Characterisation Studies of Silicon Photomultipliers", *Nuclear Instruments and Methods in Physics Research A*, vol. 620, no. 1, pp. 217-226, 2010.

[21] G. Bonanno, *et al.*, "Precision Measurements of Photon Detection Efficiency for SiPM Detectors", *Nuclear Instruments and Methods in Physics Research A*, vol. 610, pp. 93-97, 2009.

[22] G. Romeo, *et al.*, "Characterization of a 6×6-mm^2 75-μ m cell MPPC suitable for the Cherenkov Telescope Array Project", *Nuclear Instruments and Methods in Physics Research A*, vol. 826, pp. 31-38, 2016.

[23] S. K. Yang, *et al.*, "Precision Measurements of the Photon Detection Efficiency of Silicon Photomultipliers Using Two Integrated Spheres", *Optics Express*, vol. 22, no. 1, pp. 716-726, 2014.

[24] A. Asano, *et al.*, "Evaluation of silicon photomultipliers for dual-mirror Small-Sized Telescopes of Cherenkov Telescope Array",

Nuclear Instruments and Methods in Physics Research A, https://doi.org/10.1016/j.nima.2017.11.017.

[25] A. Nagai, *et al*., "SENSE: A comparison of photon detection efficiency ad optical crosstalk of various SiPM devices", *Nuclear Instruments and Methods in Physics Research A*, https://doi.org/10.1016/j.nima.2017.11.018.

[26] J. Fleury, *et al.*, "Petiroc and Citiroc: front-end ASICs for SiPM read-out and ToF applications", *Journal of Instrumentation*, vol. 9, no. 1, 2014.

[27] S. Callier, *et al.*, "EASIROC, An Easy & Versatile Readout Device for SiPM", in *Proc. TIPP*, 2001.